GSA Data Repository 2019362

van der Ploeg, R., 2019, Cenozoic carbonate burial along continental margins: Geology, v. 47, https://doi.org/10.1130/G46418.1

SUPPLEMENTARY INFORMATION

The present-day global alkalinity mass balance

A present-day, global mass balance for carbonate alkalinity was established from various literature sources under the assumption of steady state. For riverine alkalinity delivery through continental weathering ($F_{weathering}$), we use silicate weathering (F_{silw}) and carbonate weathering (F_{carbw}) estimates from Gaillardet et al. (1999), adjusted from mol C yr^{-1} to mol HCO_3^- yr^{-1} equivalents. We use the estimates from Hu and Cai (2011) to constrain alkalinity generation from anaerobic processes in organic-rich sediments deposited along continental margins ($F_{anaerobic}$), representing the sum of net denitrification and sulfate reduction associated with pyrite burial. We set the global alkalinity output flux associated with carbonate burial (F_{carbb}) equal to the sum of $F_{weathering}$ and $F_{anaerobic}$. Notably, we do not include reverse weathering as an additional sink, because present-day alkalinity removal through this process is much smaller than removal through carbonate burial (Mackenzie and Morse, 1992; Isson and Planavsky, 2018). Following Boudreau and Luo (2017), we derive present-day estimates for the pelagic carbonate burial flux ($F_{pelagic}$) from Davies and Worsley (1981) and Mackenzie and Morse (1992). We assume that $F_{pelagic}$ represents net burial rates, which implies that the amount of alkalinity removed from the pelagic oceans should be matched by alkalinity delivery from the continental margins – hence $F_{transfer}$ is set equal to $F_{pelagic}$, as in Boudreau and Luo (2017). Finally, we calculate the marginal carbonate burial flux ($F_{margins}$) as the difference between F_{carbb} and $F_{pelagic}$. See Supplementary Table 1 for an overview of these present-day parameters and

Supplementary Figure 1 for a graphical representation of the present-day global carbonate alkalinity mass balance.

Cenozoic alkalinity fluxes associated with weathering

We estimated changes in the total carbonate alkalinity delivery to the oceans associated with weathering based on inverse modelling of the marine strontium (Sr) and osmium (Os) isotope records, two well-established proxies for tracing weathering inputs to the global ocean (Ravizza and Zachos, 2003). Both the $^{87}Sr/^{86}Sr$ ratio and the $^{187}Os/^{188}Os$ ratio of seawater are controlled by inputs from continental and mantle-derived sources, with relatively well-constrained isotopic compositions at present-day. Sr is delivered to the oceans via silicate weathering, carbonate weathering, hydrothermal activity and, to a lesser extent, by diagenetic fluxes, while Os is sourced by silicate weathering, organic-rich sediment weathering, hydrothermal activity and extraterrestrial fluxes. No isotopic fractionation is associated with Sr and Os burial and consequently, changes in the $^{87}Sr/^{86}Sr$ and $^{187}Os/^{188}Os$ isotope ratios of seawater over time are governed entirely by changes in the sizes or isotopic compositions of the inputs. Building on previous studies (Delaney and Boyle, 1988; Richter and Turekian, 1993; Li and Elderfield, 2013), we use the following equations to model the $^{87}Sr/^{86}Sr$ and $^{187}Os/^{188}Os$ isotope ratios of seawater:

$$\frac{N_{Sr}}{9.43+R_{sw}}\frac{dR_{sw}}{dt} = F_{silw}\left(\frac{R_{silw}-R_{sw}}{9.43+R_{silw}}\right) + F_{carbw}\left(\frac{R_{carbw}-R_{sw}}{9.43+R_{carbw}}\right) + F_{hyd}\left(\frac{R_{hyd}-R_{sw}}{9.43+R_{hyd}}\right) + F_{dia}\left(\frac{R_{dia}-R_{sw}}{9.43+R_{dia}}\right)$$

(1)

$$\frac{N_{Os}}{7.4+R_{sw}}\frac{dR_{sw}}{dt} = F_{silw}\left(\frac{R_{silw}-R_{sw}}{7.4+R_{silw}}\right) + F_{orgw}\left(\frac{R_{orgw}-R_{sw}}{7.4+R_{orgw}}\right) + F_{hyd}\left(\frac{R_{hyd}-R_{sw}}{7.4+R_{hyd}}\right) + F_{ext}\left(\frac{R_{ext}-R_{sw}}{7.4+R_{ext}}\right)$$

(2)

where N represents the total inventory of Sr or Os in the oceans, F represents the fluxes of Sr or Os to the oceans from various sources, R represents the $^{87}Sr/^{86}Sr$ or $^{187}Os/^{188}Os$ composition of these sources and the subscripts *sw, silw, carbw, orgw, hyd, dia* and *ext* represent seawater, silicate weathering, carbonate weathering, organic-rich sediment weathering, hydrothermal, diagenetic and extraterrestrial sources, respectively. For a complete derivation of the equation for the $^{187}Os/^{188}Os$ ratio of seawater, we refer to Van der Ploeg et al. (2018) – the derivation for the $^{87}Sr/^{86}Sr$ of seawater is analogous. The factors of 9.43 and 7.4 are respectively used to derive isotopic compositions that are normalized for the natural abundances of ^{87}Sr and ^{86}Sr, and ^{187}Os and ^{188}Os (Li and Elderfield, 2013).

This system of two equations allows us to numerically solve for two unknowns – silicate and sediment weathering fluxes, in this case – if the other parameters can all be constrained. To this end, we follow a simplified version of the approach taken by Li and Elderfield (2013). The evolution of the $^{87}Sr/^{86}Sr$ and $^{187}Os/^{188}Os$ isotopic composition of seawater across the Cenozoic is well documented: for the $^{87}Sr/^{86}Sr$ ratio we use the compilation of existing data by McArthur et al. (2012), and for the $^{187}Os/^{188}Os$ ratio we use a smoothed fit to the data published in Klemm et al. (2005) and Burton (2006), updated to the age model of Nielsen et al. (2009). We force the hydrothermal Sr and Os fluxes (F_{hyd}) with a range of seafloor spreading and/or degassing rate reconstructions. We explore the use of the reconstructions of Berner (1994), Rowley (2002), Müller et al. (2008) and Van Der Meer et al. (2014), but these different forcings for F_{hyd} have a relatively minor impact on modelled changes in the various weathering fluxes (Supplementary Figure 2) and consequently we adopt the subduction zone length-based reconstructions of Van Der Meer et al. (2014) in the main text. As in previous studies (Li and Elderfield, 2013), we assume that the diagenetic Sr flux (F_{dia}) and the extraterrestrial Os flux (F_{ext}) have remained invariant over the timescale of the Cenozoic (Peucker-Ehrenbrink, 1996; Pegram and Turekian, 1999). Finally, although the seawater Sr and Os inventories have likely changed over time, on timescales of millions of years these changes are of negligible importance in comparison to the sizes of the various inputs (Li and Elderfield, 2013) and hence we assume N_{Sr} and N_{Os} to be constant.

We assume that the $^{87}Sr/^{86}Sr$ and $^{187}Os/^{188}Os$ compositions of the hydrothermal, diagenetic and extraterrestrial Sr and Os fluxes (R_{hyd}, R_{dia} and R_{ext} respectively) have remained constant at present-day values. However, the $^{87}Sr/^{86}Sr$ and $^{187}Os/^{188}Os$ compositions of the various weathering fluxes (R_{silw}, R_{carbw} and R_{orgw}) have most likely varied through time due to changing contributions from different source rock types. Because the quantitative evolution of these parameters is difficult to constrain independently (Ravizza and Zachos, 2003), we have developed several scenarios to explore the sensitivity of our results to different assumptions regarding these parameters. In Scenario 1, we assume that present-day R_{silw}, R_{carbw} and R_{orgw} values have remained unchanged during the Cenozoic, with uniform uncertainty distributions. However, this default assumption is most likely too simplistic given the range of studies that report variable isotopic compositions of weathering fluxes related to plate tectonic processes or climate events during the Cenozoic (Raymo and Ruddiman, 1992; Zachos et al., 1999; Lear et al., 2003). Therefore, we test for the effects of a progressive evolution in each of these parameters in additional scenarios. In Scenario 2 – 6, we assume a linear increase in one or more parameters from a minimum at 70 Ma towards present-day values, reflecting the impact of weathering fluxes with progressively more radiogenic $^{87}Sr/^{86}Sr$ or $^{187}Os/^{188}Os$ isotopic compositions over time. Such increases in R_{silw}, R_{carbw} and R_{orgw} would – to a first approximation – be compatible with the gradually increasing $^{87}Sr/^{86}Sr$ and $^{187}Os/^{188}Os$ isotopic compositions of seawater that have been reported for the Cenozoic (Ravizza and Zachos, 2003; Lear et al., 2003), and could potentially be related to Himalayan uplift (Colleps et al., 2018). In Scenario 2, we increase the $^{87}Sr/^{86}Sr$ composition of silicate weathering linearly from 0.7183 at

70 Ma to 0.7203 at present-day, while in Scenario 3, we increase the $^{87}Sr/^{86}Sr$ composition of carbonate weathering increase linearly from 0.7057 at 70 Ma to 0.7077 at present-day. In Scenario 4, we increase the $^{187}Os/^{188}Os$ composition of silicate weathering linearly from 0.60 at 70 Ma to 1.05 at present-day, and in Scenario 5, we increase the $^{187}Os/^{188}Os$ composition of organic-rich sediment weathering linearly from 1.00 at 70 Ma to 1.78 at present-day. Finally, in Scenario 6, we combine the increase in the $^{87}Sr/^{86}Sr$ composition of silicate weathering as in Scenario 2 with the increase in the $^{187}Os/^{188}Os$ composition of organic-rich sediment weathering as in Scenario 5, because these parameters are thought to have a large impact on weathering flux estimates (Peucker-Ehrenbrink and Ravizza, 2000; Li et al., 2009). Together, Scenarios 1 – 6 provide solutions for these weathering fluxes under a range of probable isotopic compositions.

Finally, we adopt the assumption that carbonate weathering (F_{carbw}) and organic-rich sediment weathering (F_{orgw}) are proportional to each other on a global scale, and that these two fluxes can be combined as global sediment weathering (F_{sedw}) (Derry and France-Lanord, 1996; Li and Elderfield, 2013). This leaves us with only two remaining unknowns, F_{silw} and F_{sedw}, which can be solved numerically for the Cenozoic with the above equations. The total carbonate alkalinity flux from continental weathering ($F_{weathering}$) is then given by:

$$F_{weathering} = F_{silw} + F_{sedw} \quad (3)$$

in which the fluxes are calculated relative to their present-day values.

See Supplementary Table 1 for an overview of all present-day parameter values used for Sr and Os cycle modelling and Supplementary Table 2 for an overview of the different scenarios described above. The model results for these scenarios are shown in Supplementary

Figure 3 – 5. We use minimum, mean and maximum estimates based on the full range of these scenarios (Supplementary Figure 6) for our main $F_{weathering}$ estimates shown in Figure 1.

Cenozoic alkalinity fluxes associated with anaerobic processes in marginal sediments

Because alkalinity addition from $F_{anaerobic}$ is much smaller than $F_{weathering}$ (Hu and Cai, 2011) and the temporal evolution of $F_{anaerobic}$ is difficult to constrain, we assume that $F_{anaerobic}$ has remained constant over the Cenozoic. To accommodate associated uncertainties we use the full range of estimates reported by Hu and Cai (2011), including alkalinity inputs from organic carbon preservation and pyrite burial in coastal vegetated sediments. The resulting estimates are shown in Figure 1.

Cenozoic alkalinity fluxes associated with pelagic carbonate burial

The alkalinity output flux associated with carbonate burial in the pelagic oceans ($F_{pelagic}$) is calculated following Boudreau and Luo (2017). Here, we take the retrodicted pelagic carbonate burial rates of Boudreau and Luo (2017) (in mol $CaCO_3$ / Myr) that were driven by the global Cenozoic CCD curve of Lyle et al. (2008) and the Pacific CCD curve for the last 50 Myr of Pälike et al. (2012), and adjust their values to alkalinity equivalents (in mol HCO_3^- / Myr). We also incorporate uncertainties in the size of the present-day pelagic carbonate burial flux by using minimum and maximum estimates based on Davies and Worsley (1981) and Mackenzie and Morse (1992). The resulting estimates are shown in Figure 1.

Cenozoic alkalinity fluxes associated with marginal carbonate burial

With $F_{weathering}$, $F_{anaerobic}$ and $F_{pelagic}$ constrained, the alkalinity output flux associated with carbonate burial along continental margins ($F_{margins}$) can be calculated using a mass balance for global carbonate alkalinity:

$$\frac{dN_{Alk}}{dt} = F_{weathering} + F_{anaerobic} - F_{margins} - F_{pelagic} \quad (4)$$

in which N_{Alk} represents the total inventory of carbonate alkalinity in the oceans.

We calculate $F_{margins}$ values with propagation of the uncertainties for $F_{weathering}$, $F_{anaerobic}$ and $F_{pelagic}$ described above using the root of the mean square errors. We assess the impact of potential temporal changes in N_{Alk} using the Cenozoic carbonate alkalinity reconstructions of Boudreau et al. (2019) to account for any imbalances in the global inputs and outputs of carbonate alkalinity (Supplementary Figure 7). We convert these modelled carbonate alkalinity concentrations from mmol HCO_3^- kg^{-1} to a total carbonate alkalinity inventory in mol HCO_3^- by assuming a seawater density of 1.035 kg L^{-1} and a global ocean volume of 1.33 x 10^{21} L following Charette and Smith (2000). Importantly, the maximum imbalance calculated from the reconstructions of Boudreau et al. (in revision) is up to two orders of magnitude smaller than the sizes of the alkalinity fluxes, so the effect of any changes over time in N_{Alk} on $F_{margins}$ is negligible (Supplementary Figure 7). Hence, we assume N_{alk} to be constant and dN_{alk}/dt to be zero for our main $F_{margins}$ estimates shown in Figure 1.

REFERENCES CITED

Allègre, C.J., and Luck, J.M., 1980, Osmium isotopes as petrogenetic and geological tracers: Earth and Planetary Science Letters, v. 48, p. 148–154, doi:10.1016/0012-821X(80)90177-6.

Bach, W., and Humphris, S.E., 1999, Relationship between the Sr and O isotope compositions of hydrothermal fluids and the spreading and magma-supply rates at oceanic spreading centers: Geology, v. 27, p. 1067–1070, doi:10.1130/0091-7613(1999)027<1067:RBTSAO>2.3.CO;2.

Berner, R.A., 1994, GEOCARB II; a revised model of atmospheric CO_2 over Phanerozoic time: American Journal of Science, v. 294, p. 56–91, doi:10.2475/ajs.294.1.56.

Boudreau, B.P., and Luo, Y., 2017, Retrodiction of secular variations in deep-sea $CaCO_3$ burial during the Cenozoic: Earth and Planetary Science Letters, v. 474, p. 1–12, doi:10.1016/j.epsl.2017.06.005.

Boudreau, B.P., Middelburg, J.J., Sluijs, A., and Van der Ploeg, R., 2019, Secular variations in the carbonate chemistry of the oceans over the Cenozoic: Earth and Planetary Science Letters, v. 512, p. 194–206, doi:10.1016/j.epsl.2019.02.004.

Burton, K.W., 2006, Global weathering variations inferred from marine radiogenic isotope records: Journal of Geochemical Exploration, v. 88, p. 262–265, doi:10.1016/j.gexplo.2005.08.052.

Charette, M., and Smith, W., 2010, The Volume of Earth's Ocean: Oceanography, v. 23, p. 112–114, doi:10.5670/oceanog.2010.51.

Colleps, C.L., McKenzie, N.R., Stockli, D.F., Hughes, N.C., Singh, B.P., Webb, A.A.G., Myrow, P.M., Planavsky, N.J., and Horton, B.K., 2018, Zircon (U-Th)/He Thermochronometric Constraints on Himalayan Thrust Belt Exhumation, Bedrock Weathering, and Cenozoic Seawater Chemistry: Geochemistry, Geophysics, Geosystems, v. 19, p. 257–271, doi:10.1002/2017GC007191.

Davies, T.A., and Worsley, T.R., 1981, Paleoenvironmental implications of oceanic carbonate sedimentation rates, *in* The Deep Sea Drilling Project: A Decade of Progress, SEPM (Society for Sedimentary Geology), p. 169–179, doi:10.2110/pec.81.32.0169.

Delaney, M.L., and Boyle, E.A., 1988, Tertiary paleoceanic chemical variability: Unintended consequences of simple geochemical models: Paleoceanography, v. 3, p. 137–156, doi:10.1029/PA003i002p00137.

Derry, L.A., and France-Lanord, C., 1996, Neogene Himalayan weathering history and river

$^{87}Sr/^{86}Sr$: impact on the marine Sr record: Earth and Planetary Science Letters, v. 142, p. 59–74, doi:10.1016/0012-821X(96)00091-X.

Elderfield, H., and Gieskes, J.M., 1982, Sr isotopes in interstitial waters of marine sediments from Deep Sea Drilling Project cores: Nature, v. 300, p. 493.

Gaillardet, J., Dupré, B., Louvat, P., and Allègre, C.J., 1999, Global silicate weathering and CO_2 consumption rates deduced from the chemistry of large rivers: Chemical Geology, v. 159, p. 3–30, doi:10.1016/S0009-2541(99)00031-5.

Hu, X., and Cai, W.J., 2011, An assessment of ocean margin anaerobic processes on oceanic alkalinity budget: Global Biogeochemical Cycles, v. 25, p. 1–11, doi:10.1029/2010GB003859.

Isson, T.T., and Planavsky, N.J., 2018, Reverse weathering as a long-term stabilizer of marine pH and planetary climate: Nature, v. 560, p. 471–475, doi:10.1038/s41586-018-0408-4.

Klemm, V., Levasseur, S., Frank, M., Hein, J.R., and Halliday, A.N., 2005, Osmium isotope stratigraphy of a marine ferromanganese crust: Earth and Planetary Science Letters, v. 238, p. 42–48, doi:10.1016/j.epsl.2005.07.016.

Lear, C.H., Elderfield, H., and Wilson, P.A., 2003, A Cenozoic seawater Sr/Ca record from benthic foraminiferal calcite and its application in determining global weathering fluxes: Earth and Planetary Science Letters, v. 208, p. 69–84, doi:10.1016/S0012-821X(02)01156-1.

Li, G., and Elderfield, H., 2013, Evolution of carbon cycle over the past 100 million years: Geochimica et Cosmochimica Acta, v. 103, p. 11–25, doi:10.1016/j.gca.2012.10.014.

Li, G., Ji, J., Chen, J., and Kemp, D.B., 2009, Evolution of the Cenozoic carbon cycle: The roles of tectonics and CO_2 fertilization: Global Biogeochemical Cycles, v. 23, p. 1–11, doi:10.1029/2008GB003220.

Lyle, M., Barron, J., Bralower, T.J., Huber, M., Lyle, A.O., Ravelo, A.C., Rea, D.K., and

Wilson, P.A., 2008, Pacific ocean and cenozoic evolution of climate: Reviews of Geophysics, v. 46, p. 1–47, doi:10.1029/2005RG000190.

Mackenzie, F.T., and Morse, J.W., 1992, Sedimentary carbonates through Phanerozoic time: Geochimica et Cosmochimica Acta, v. 56, p. 3281–3295, doi:10.1016/0016-7037(92)90305-3.

McArthur, J.M., Howarth, R.J., and Shields, G.A., 2012, Strontium Isotope Stratigraphy, *in* The Geologic Time Scale, Felix M. Gradstein, James G. Ogg, Mark Schmitz and Gabi Ogg, p. 127–144, doi:10.1016/B978-0-444-59425-9.00007-X.

Van Der Meer, D.G., Zeebe, R.E., van Hinsbergen, D.J.J., Sluijs, A., Spakman, W., and Torsvik, T.H., 2014, Plate tectonic controls on atmospheric CO_2 levels since the Triassic: Proceedings of the National Academy of Sciences of the United States of America, v. 111, p. 4380–5, doi:10.1073/pnas.1315657111.

Müller, R.D., Sdrolias, M., Gaina, C., Steinberger, B., and Heine, C., 2008, Long-Term Sea-Level Fluctuations Driven by Ocean Basin Dynamics: Science, v. 319, p. 1357–1362, doi:10.1126/science.1151540.

Nielsen, S.G., Mar-Gerrison, S., Gannoun, A., LaRowe, D., Klemm, V., Halliday, A.N., Burton, K.W., and Hein, J.R., 2009, Thallium isotope evidence for a permanent increase in marine organic carbon export in the early Eocene: Earth and Planetary Science Letters, v. 278, p. 297–307, doi:10.1016/j.epsl.2008.12.010.

Oxburgh, R., 2001, Residence time of osmium in the oceans: Geochemistry, Geophysics, Geosystems, v. 2, p. 2954–2976, doi:http://dx.doi.org/10.1002/ggge.20188.

Pälike, H. et al., 2012, A Cenozoic record of the equatorial Pacific carbonate compensation depth: Nature, v. 488, p. 609–614, doi:10.1038/nature11360.

Palmer, M.R., and Edmond, J.M., 1989, The strontium isotope budget of the modern ocean: Earth and Planetary Science Letters, v. 92, p. 11–26.

Pegram, W.J., and Turekian, K.K., 1999, The osmium isotopic composition change of Cenozoic sea water as inferred from a deep-sea core corrected for meteoritic contributions: Geochimica et Cosmochimica Acta, v. 63, p. 4053–4058, doi:10.1016/S0016-7037(99)00308-7.

Peucker-Ehrenbrink, B., 1996, Accretion of extraterrestrial matter during the last 80 million years and its effect on the marine osmium isotope record: Geochimica et Cosmochimica Acta, v. 60, p. 3187–3196, doi:10.1016/0016-7037(96)00161-5.

Peucker-Ehrenbrink, B., and Jahn, B.-M., 2001, Rhenium-osmium isotope systematics and platinum group element concentrations: Loess and the upper continental crust: Geochemistry, Geophysics, Geosystems, v. 2, p. 2001GC000172.

Peucker-Ehrenbrink, B., and Ravizza, G.E., 2000, The marine osmium isotope record: Terra Nova, v. 12, p. 205–219, doi:10.1046/j.1365-3121.2000.00295.x.

Van der Ploeg, R., Selby, D., Cramwinckel, M.J., Li, Y., Bohaty, S.M., Middelburg, J.J., and Sluijs, A., 2018, Middle Eocene greenhouse warming facilitated by diminished weathering feedback: Nature Communications, v. 9, p. 2877, doi:10.1038/s41467-018-05104-9.

Ravizza, G.E., and Zachos, J.C., 2003, Records of Cenozoic Ocean Chemistry: Treatise on Geochemistry, v. 6, p. 551–581, doi:10.1016/B978-0-08-095975-7.00620-3.

Raymo, M.E., and Ruddiman, W.F., 1992, Tectonic forcing of late Cenozoic climate: Nature, v. 359, p. 117–122.

Richter, F.M., and Turekian, K.K., 1993, Simple models for the geochemical response of the ocean to climatic and tectonic forcing: Earth and Planetary Science Letters, v. 119, p. 121–131, doi:10.1016/0012-821X(93)90010-7.

Rowley, D.B., 2002, Rate of plate creation and destruction: 180 Ma to present: Geological Society of America Bulletin, v. 114, p. 927–933, doi:10.1130/0016-

7606(2002)114<0927:ROPCAD>2.0.CO;2.

Zachos, J.C., Opdyke, B.N., Quinn, T.M., Jones, C.E., and Halliday, A.N., 1999, Early cenozoic glaciation, antarctic weathering, and seawater $^{87}Sr/^{86}Sr$: is there a link? Chemical Geology, v. 161, p. 165–180, doi:Doi: 10.1016/s0009-2541(99)00085-6.

Supplementary Table 1: Overview of all parameters used in alkalinity, Sr and Os cycle modelling. All values are present-day values taken from the literature or fitted to match the present-day steady state observations.

Parameter	Parameter description	Value	Reference and Comments
Alkalinity			
F_{silw}	Silicate weathering flux of alkalinity to oceans	11.7 x 10^{18} mol/Myr	Gaillardet et al. (1999)
F_{carbw}	Carbonate weathering flux of alkalinity to oceans	24.6 x 10^{18} mol/Myr	Gaillardet et al. (1999)
$F_{weathering}$	Continental weathering flux of alkalinity to oceans	36.3 x 10^{18} mol/Myr	Calculated by adding F_{silw} and F_{carbw}
$F_{anaerobic}$	Alkalinity production through anaerobic processes along continental margins	4 – 6 x 10^{18} mol/Myr	Hu and Cai (2011), taken as the sum of net denitrification and pyrite burial fluxes
F_{carbb}	Carbonate burial flux of alkalinity from oceans	41.3 x 10^{18} mol/Myr	Calculated by adding $F_{weathering}$ and $F_{anaerobic}$, assuming steady state
$F_{pelagic}$	Pelagic carbonate burial flux of alkalinity from oceans	24 – 30 x 10^{18} mol/Myr	Boudreau and Luo (2017), following Davies and Worsley (1981) and Mackenzie and Morse (1992)
$F_{margins}$	Marginal carbonate burial flux of alkalinity from oceans	11.3 – 17.3 x 10^{18} mol/Myr	Calculated by subtracting $F_{pelagic}$ from F_{carbb}, assuming steady state
Sr			
N	Sr inventory in oceans	1.25 x 10^{17} mol	Palmer and Edmond (1989)
F_{silw}	Silicate weathering flux of Sr to oceans	1.05 x 10^{16} mol/Myr	Li and Elderfield (2013)
F_{carbw} (F_{sedw})	Carbonate weathering flux of Sr to oceans	2.35 x 10^{16} mol/Myr	Li and Elderfield (2013)
F_{hyd}	Hydrothermal flux of Sr to oceans	1.46 x 10^{16} mol/Myr	Li and Elderfield (2013), taken as the sum of the island basalt weathering and hydrothermal fluxes
F_{dia}	Diagenetic flux of Sr to oceans	7.80 x 10^{15} mol/Myr	Calculated to arrive at steady state of R_{sw} = 0.709175
R_{silw}	$^{87}Sr/^{86}Sr$ composition of silicate weathering flux	0.7203	Li and Elderfield (2013), following Li et al. (2009)
R_{carbw}	$^{87}Sr/^{86}Sr$ composition of carbonate weathering flux	0.7077	Li and Elderfield (2013), following Li et al. (2009)
R_{hyd}	$^{87}Sr/^{86}Sr$ composition of hydrothermal flux	0.7037	Li and Elderfield (2013), following Bach and Humphris (1999)
R_{dia}	$^{87}Sr/^{86}Sr$ composition of diagenetic flux	0.7084	Li and Elderfield (2013), following Elderfield and Gieskes (1982)
R_{sw}	$^{87}Sr/^{86}Sr$ composition of seawater	0.709175	McArthur et al. (2012)
Os			
N	Os inventory in oceans	6.83 x 10^{7} mol	Oxburgh (2001)
F_{silw}	Silicate weathering flux of Os to oceans	551 x 10^{6} mol/Myr	Li and Elderfield (2013), following Li et al. (2009)
F_{orgw} (F_{sedw})	Organic-rich sediment weathering flux of Os to oceans	1119 x 10^{6}mol/yr	Li and Elderfield (2013), following Li et al. (2009)
F_{hyd}	Hydrothermal flux of Os to oceans	710 x 10^{6} mol/yr	Li and Elderfield (2013), taken as the sum of the island basalt weathering and hydrothermal fluxes
F_{ext}	Extraterrestrial flux of Os to oceans	260 x 10^{6} mol/yr	Calculated to arrive at steady state of R_{sw} = 1.02
R_{silw}	$^{187}Os/^{188}Os$ composition of silicate weathering flux	1.05	Li and Elderfield (2013), following Peucker-Ehrenbrink and Jahn (2001)
R_{orgw}	$^{187}Os/^{188}Os$ composition of organic-rich sediment weathering flux	1.78	Li and Elderfield (2013), following Li et al. (2009)
R_{hyd}	$^{187}Os/^{188}Os$ composition of hydrothermal flux	0.126	Li and Elderfield (2013), following Allègre and Luck (1980)
R_{ext}	$^{187}Os/^{188}Os$ composition of extraterrestrial flux	0.126	Li and Elderfield (2013), following Allègre and Luck (1980)
R_{sw}	$^{187}Os/^{188}Os$ composition of seawater	1.02	Klemm et al. (2005), Burton (2006), Nielsen et al. (2009), obtained using a smoothing spline

Supplementary Table 2: Overview of the uncertainties incorporated in the weathering reconstructions and the different scenarios for the $^{87}Sr/^{86}Sr$ and $^{187}Os/^{188}Os$ compositions of the various weathering fluxes. Scenario 1 represents the default scenario, while in Scenario 2 – 6 linear a linear increase in one or more parameter values is prescribed from 70 Ma to present-day. For these additional scenarios, only the parameters that are different with respect to Scenario 1 are listed.

Scenario	Parameter	Present-day value	Uncertainty	Prescribed 70 Ma value	Reference and Comments
Scenario 1: all present-day values unchanged					All other parameters as in Supplementary Table 1
Sr	R_{silw}	0.7203	± 0.001	0.7203	Uniform uncertainty
	R_{carbw}	0.7077	± 0.001	0.7077	Uniform uncertainty
Os	R_{silw}	1.05	± 0.1	1.05	Uniform uncertainty
	R_{orgw}	1.78	± 0.1	1.78	Uniform uncertainty
Scenario 2: increasing $^{87}Sr/^{86}Sr$ of silicate weathering	R_{silw}	0.7203	-	0.7183	Linear increase from 70 Ma to 0 Ma
Scenario 3: increasing $^{87}Sr/^{86}Sr$ of carbonate weathering	R_{carbw}	0.7077	-	0.7057	Linear increase from 70 Ma to 0 Ma
Scenario 4: increasing $^{187}Os/^{188}Os$ of silicate weathering	R_{silw}	1.05	-	0.60	Linear increase from 70 Ma to 0 Ma
Scenario 5: increasing $^{187}Os/^{188}Os$ of organic-rich sediment weathering	R_{orgw}	1.78	-	1.00	Linear increase from 70 Ma to 0 Ma
Scenario 6: increasing R_{silw} $^{87}Sr/^{86}Sr$ and R_{orgw} $^{187}Os/^{188}Os$					
Sr	R_{silw}	0.7203	-	0.7183	Linear increase from 70 Ma to 0 Ma
Os	R_{orgw}	1.78	-	1.00	Linear increase from 70 Ma to 0 Ma

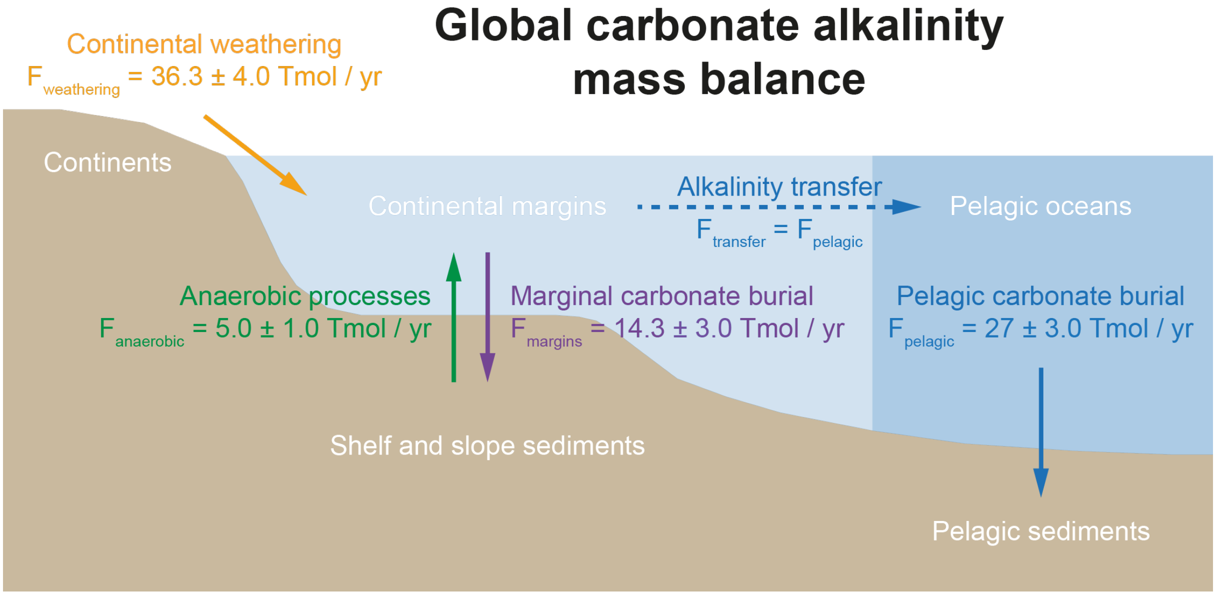

Supplementary Figure 1: Schematic representation of the present-day global carbonate alkalinity mass balance. Values are expressed as Tmol HCO_3^- yr^{-1} and sources are listed in Supplementary Table 1.

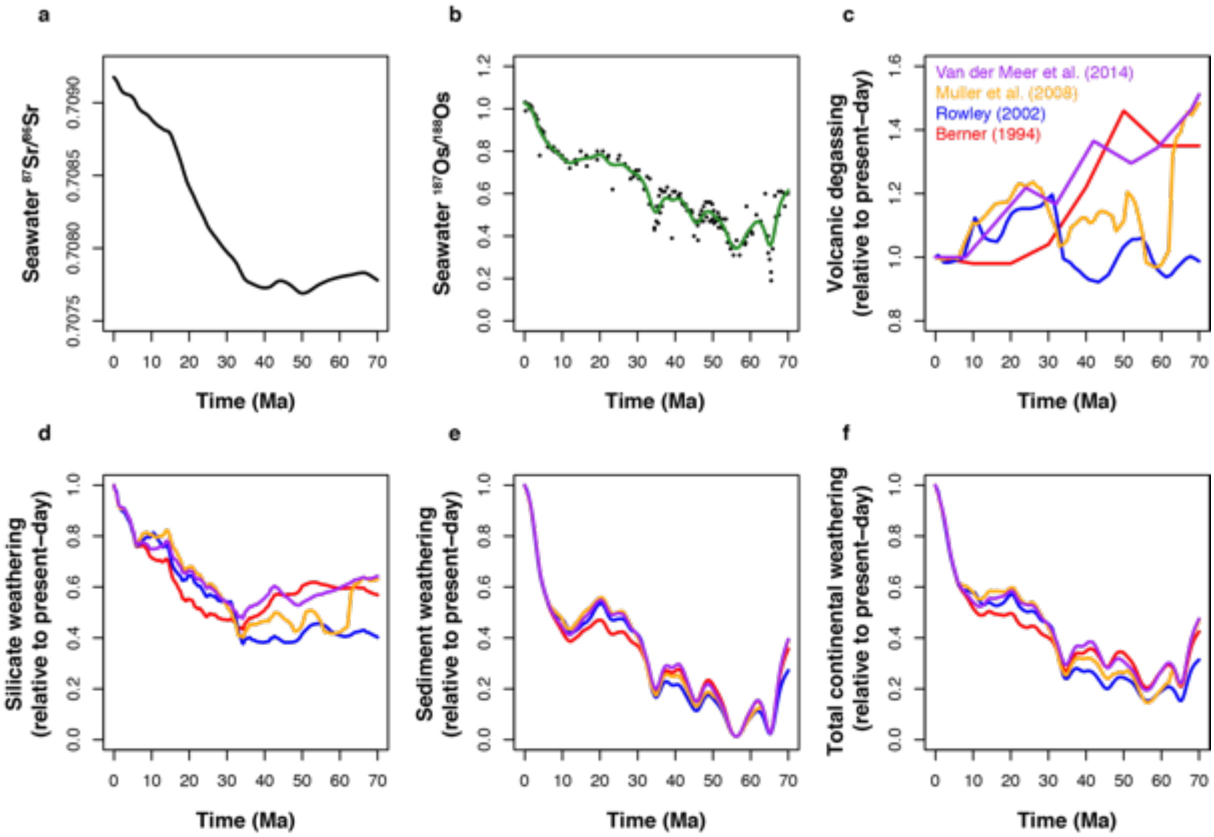

Supplementary Figure 2: Sensitivity of the modelled continental weathering rates to different hydrothermal flux forcings. a, Seawater $^{87}Sr/^{86}Sr$ compilation of McArthur et al. (2012) (in black). **b,** Seawater $^{187}Os/^{188}Os$ records of Klemm et al. (2005) and Burton (2006), updated to the age model of Nielsen et al. (2009). The green line represents the smoothed fit used in our model calculations. **c,** Volcanic degassing rates relative to present-day values used as forcings for the hydrothermal Sr and Os fluxes (F_{hyd}). Shown are the reconstructions of Berner (1994) (in red), Rowley (2002), Müller et al. (2008) (in orange) and Van Der Meer et al. (2014) (in purple). **d,** Modelled silicate weathering rates (F_{silw}) and **e,** sediment weathering rates (F_{sedw}) relative to present-day values resulting from the forcings in (a), (b) and (c) and the parameters of Scenario 1. **f,** Modelled total continental weathering rates ($F_{weathering}$) relative to present-day values, obtained by proportionally adding F_{silw} and F_{sedw} as in (d) and (e).

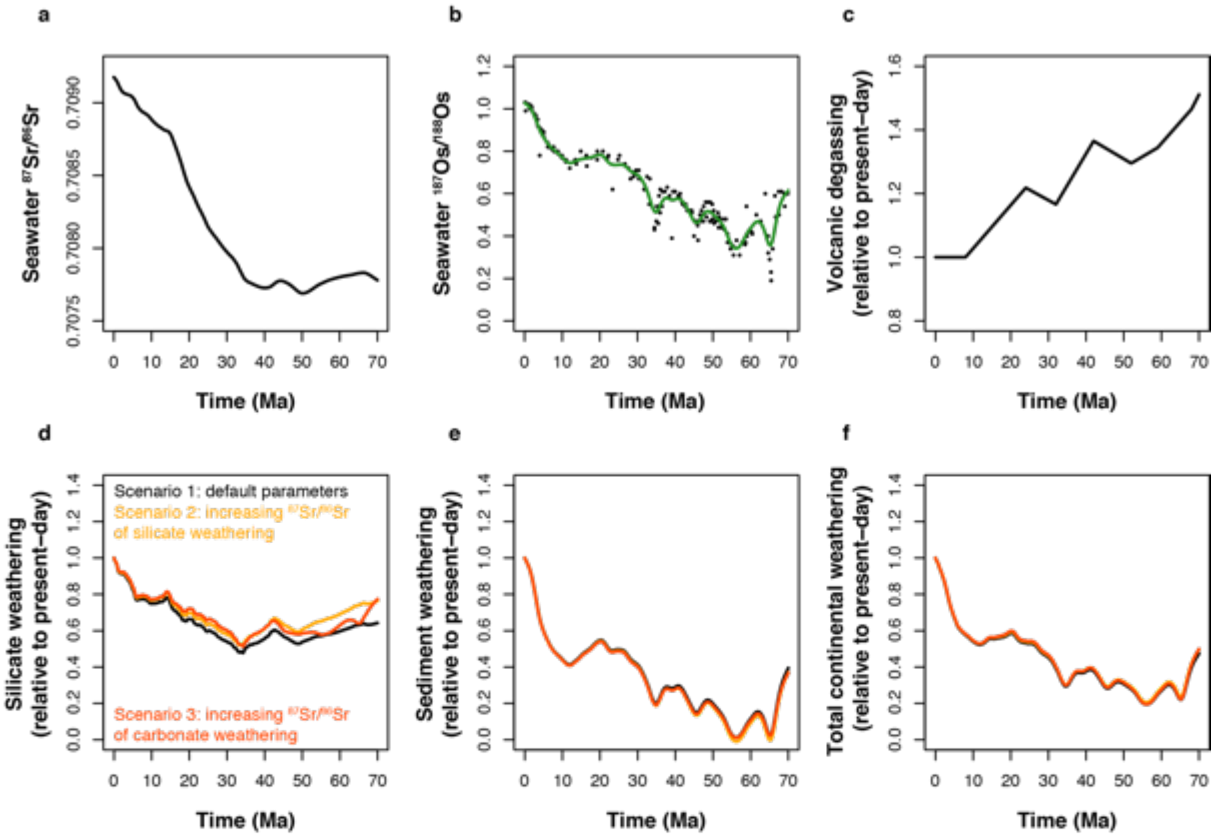

Supplementary Figure 3: Sensitivity of the modelled continental weathering rates to changes in isotopic compositions of weathering sources. a, Seawater $^{87}Sr/^{86}Sr$ compilation of McArthur et al. (2012) (in black). **b,** Seawater $^{187}Os/^{188}Os$ records of Klemm et al. (2005) and Burton (2006), updated to the age model of Nielsen et al. (2009). The green line represents the smoothed fit used in our model calculations. **c,** Volcanic degassing rates relative to present-day values, based on subduction zone length-based degassing rate reconstructions (Van Der Meer et al., 2014). **d,** Modelled silicate weathering rates (F_{silw}) and **e,** carbonate and organic-rich sediment weathering rates (F_{sedw}) relative to present-day values, resulting from the forcings shown in (a), (b) and (c) and the parameters of Scenario 1 (in black), Scenario 2 (in orange) and Scenario 3 (in red). **f,** Modelled total continental weathering rates ($F_{weathering}$) relative to present-day values, obtained by proportionally adding F_{silw} and F_{sedw} as in (d) and (e).

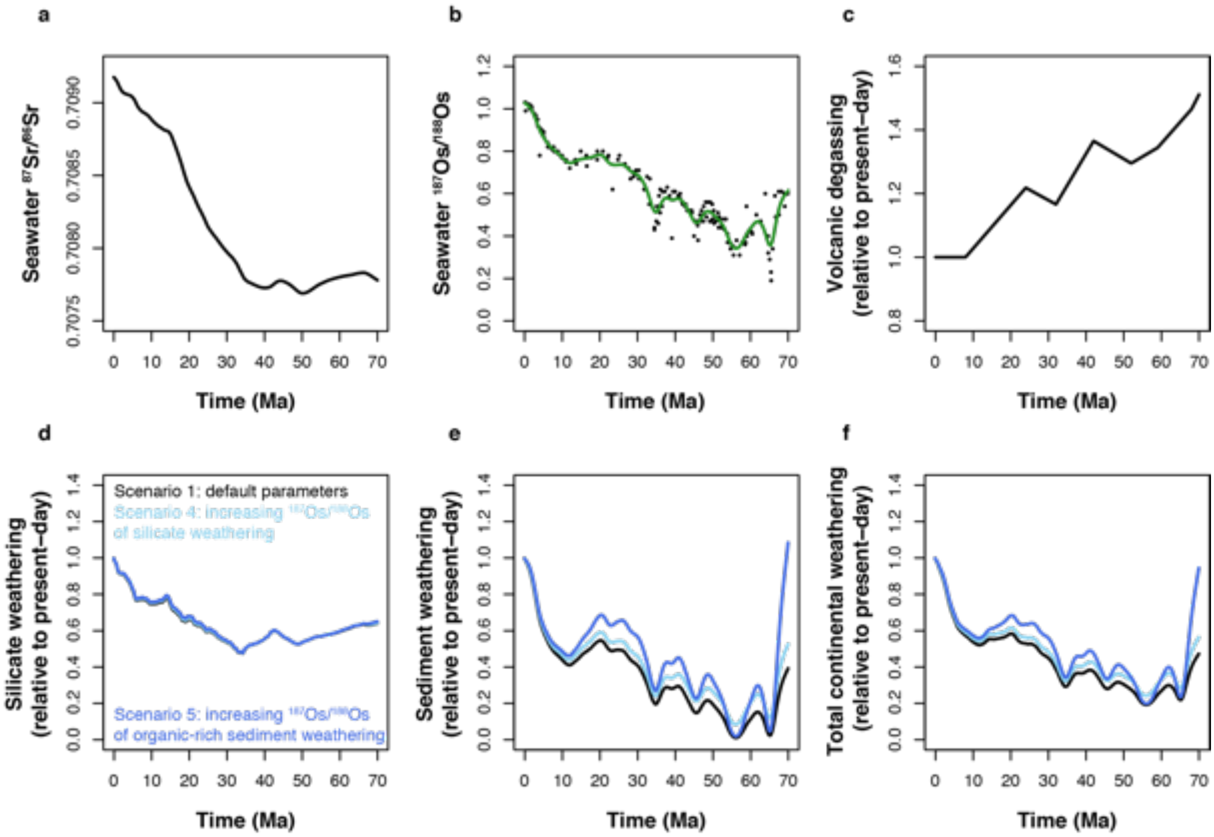

Supplementary Figure 4: Sensitivity of the modelled continental weathering rates to changes in isotopic compositions of weathering sources. a, Seawater $^{87}Sr/^{86}Sr$ compilation of McArthur et al. (2012) (in black). **b,** Seawater $^{187}Os/^{188}Os$ records of Klemm et al. (2005) and Burton (2006), updated to the age model of Nielsen et al. (2009). The green line represents the smoothed fit used in our model calculations. **c,** Volcanic degassing rates relative to present-day values, based on subduction zone length-based degassing rate reconstructions (Van Der Meer et al., 2014). **d,** Modelled silicate weathering rates (F_{silw}) and **e,** carbonate and organic-rich sediment weathering rates (F_{sedw}) relative to present-day values, resulting from the forcings shown in (a), (b) and (c) and the parameters of Scenario 1 (in black), Scenario 4 (in light blue) and Scenario 5 (in dark blue). **f,** Modelled total continental weathering rates ($F_{weathering}$) relative to present-day values, obtained by proportionally adding F_{silw} and F_{sedw} as in (d) and (e).

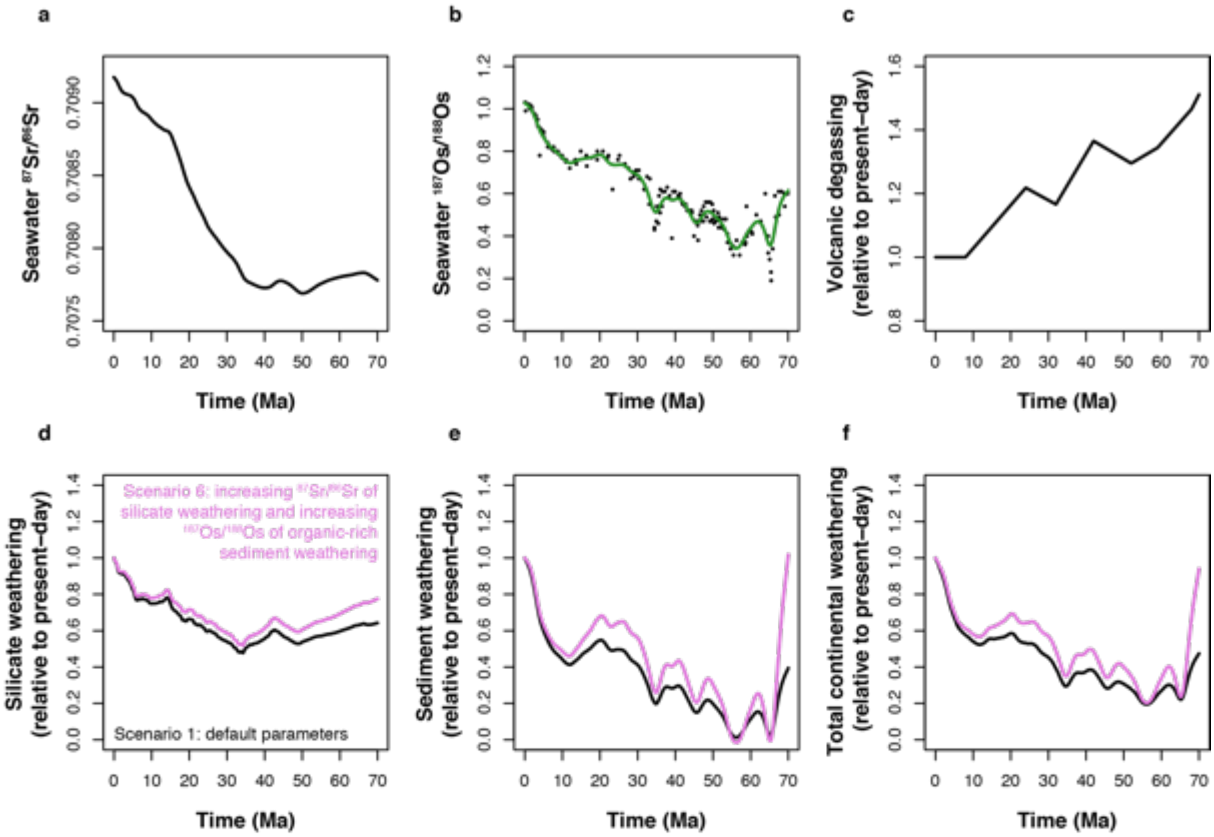

Supplementary Figure 5: Sensitivity of the modelled continental weathering rates to changes in isotopic compositions of weathering sources. a, Seawater $^{87}Sr/^{86}Sr$ compilation of McArthur et al. (2012) (in black). **b,** Seawater $^{187}Os/^{188}Os$ records of Klemm et al. (2005) and Burton (2006), updated to the age model of Nielsen et al. (2009). The green line represents the smoothed fit used in our model calculations. **c,** Volcanic degassing rates relative to present-day values, based on subduction zone length-based degassing rate reconstructions (Van Der Meer et al., 2014). **d,** Modelled silicate weathering rates (F_{silw}) and **e,** carbonate and organic-rich sediment weathering rates (F_{sedw}) relative to present-day values, resulting from the forcings shown in (a), (b) and (c) and the parameters of Scenario 1 (in black) and Scenario 6 (in purple). **f,** Modelled total continental weathering rates ($F_{weathering}$) relative to present-day values, obtained by proportionally adding F_{silw} and F_{sedw} as in (d) and (e).

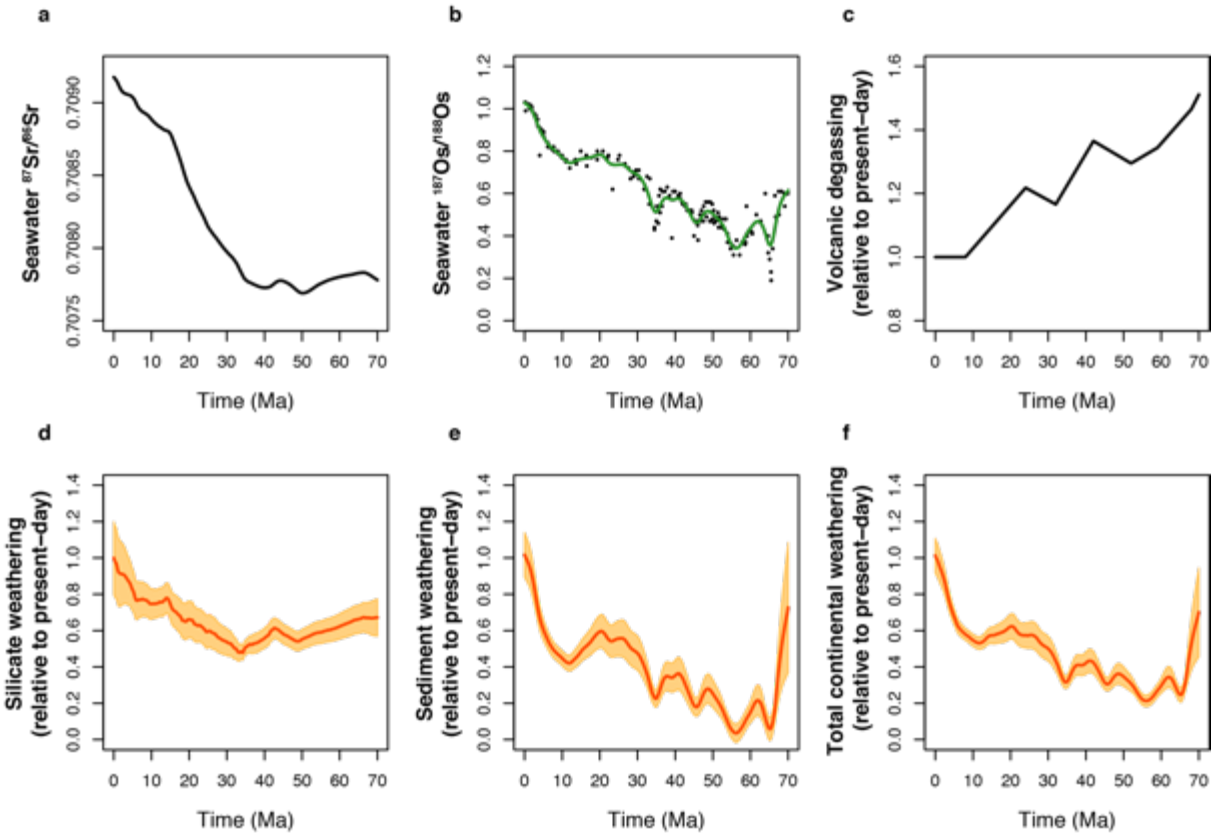

Supplementary Figure 6: Summary of scenarios for modelled continental weathering rates for the Cenozoic. a, Seawater $^{87}Sr/^{86}Sr$ compilation of McArthur et al. (2012) (in black). **b,** Seawater $^{187}Os/^{188}Os$ records of Klemm et al. (2005) and Burton (2006), updated to the age model of Nielsen et al. (2009). The green line represents the smoothed fit used in our model calculations. **c,** Volcanic degassing rates relative to present-day values, based on subduction zone length-based degassing rate reconstructions (Van Der Meer et al., 2014). **d,** Modelled silicate weathering rates (F_{silw}) and **e,** carbonate and organic-rich sediment weathering rates (F_{sedw}) relative to present-day values. The shaded areas correspond to the minimum and maximum estimates based on the full range of Scenarios 1 – 6 as in Supplementary Figure 3 – 5, with the red line representing the mean of these estimates. **f,** Modelled total continental weathering rates ($F_{weathering}$) relative to present-day values, obtained by proportionally adding F_{silw} and F_{sedw} as in (d) and (e).

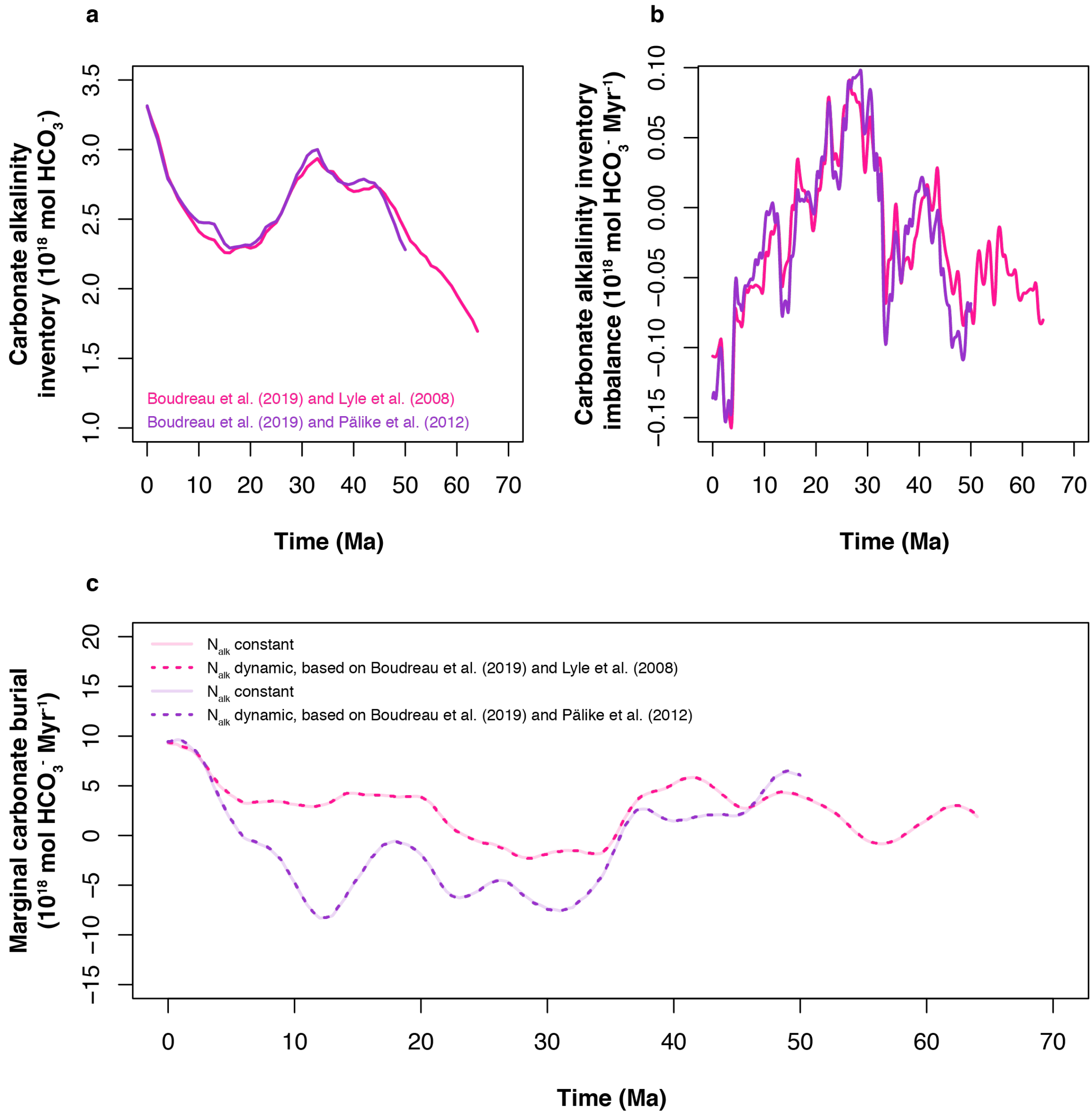

Supplementary Figure 7: Sensitivity of marginal carbonate burial to changes in the alkalinity inventory of the global ocean. a, Global carbonate alkalinity inventory (N_{alk}) as estimated by Boudreau et al. (in revision), based on the Lyle et al. (2008) CCD (in pink) or the Pälike et al. (2012) CCD (in purple). **b,** Imbalance in the global carbonate alkalinity inventory, obtained as dN_{alk}/dt from the estimates in (a). **c,** Marginal carbonate burial rates ($F_{margins}$) calculated by assuming constant N_{alk} (solid lines) or dynamic N_{alk} (dashed lines) following the estimates in (a) and (b). Total continental weathering rates ($F_{weathering}$) are based on the parameters of Scenario 1 and the pelagic burial rates ($F_{pelagic}$) are based either on the Lyle et al.

CCD (pink) or the Pälike et al. CCD (purple). The difference between constant and dynamic N_{alk} is negligible and hence the solid and dashed lines overlap.